Consolidation of Magnesium Alloys Using Cold Spray

Theresa Dillon, Victor Champagne, and Matthew Trexler
US Army Research Laboratory

Abstract

The cold spray process is a powder consolidation method that is capable of producing fully dense coating and bulk materials using accelerated particles that are deformed during high velocity impact onto a substrate. The technique is used to repair magnesium components that have been damaged either mechanically or due to corrosion. The common repair involves spraying Aluminum (Mg) onto these components as the Al not only allows for dimensional restoration but adds additional corrosion protection as well. However, recent advances in corrosion resistant magnesium alloys have led to research regarding the consolidation of these alloy powders via cold spray. This work summarizes progress that has been made in consolidating magnesium alloys such as AZ31B, WE43, and others to near full density. Results indicate that cold spray can be used as a novel additive manufacturing techniques for making bulk magnesium alloy parts.

Introduction

Due to the low densities and high strength-to-weight ratios, magnesium (Mg) alloys are desirable for many industrial and military applications. The, magnesium-aluminum-zinc alloys are a good example of an alloy having this high strength to weight ratio. Aluminum (Al) addition to this alloy increases desirable properties such as increasing yield strength, ultimate tensile strength, corrosion resistance, and oxidation resistance while the zinc addition increases strength and reduces ductility (1). Depositing metal powders onto substrates to form bulk materials using cold spray technology has several advantages over other methodologies. The melting temperature of the material is not reached during cold spray, which essentially cold works the solid state particles increasing the hardness (2). The typical cold spray deposition process involves accelerating metal particles into the surface layer of a substrate at high speeds (3). Figure 1 shows a simplified diagram of a typical cold spray set-up. As these particles impact the substrate surface both the particle and the surface are deformed plastically, thereby allowing the particle to adhere mechanically to the surface. Particular note of the converging-diverging nozzle should be taken; this design provides supersonic speeds, which the particles require for deposition, from the expanding heated gas as it leaves the nozzle (4).

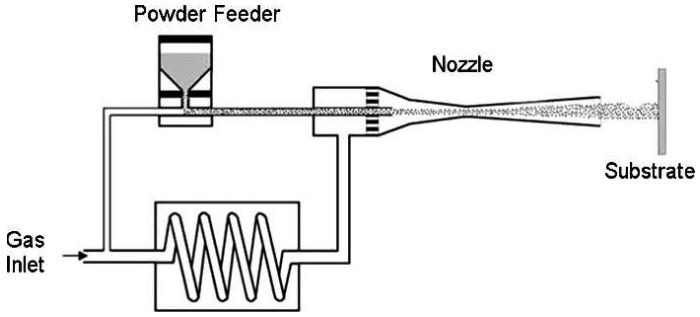

Figure 1 Schematic of the Army Research Laboratories cold spray set-up. (2)

This work focuses on the effects of driving gas temperature on the morphology and hardness. During cold spray each layer of deposited particles impacts the previously deposited layer creating a gradient of characteristics. Some of these characteristics are examined here. The effects of main gas temperature on AZ31B consolidation using cold spray methods were evaluated by measuring percent porosity, percent undeformed particles, deposition efficiency (DE) and Vickers hardness.

Experimental Procedure

Process modeling

A model previously developed by Helfritch etal was used to predict the optimal powder size required to optimize the cold spray parameters in terms of deposition efficiency which is a measure of process waste. The model relies on assumptions based on material properties such as density, modulus and yield strength and has been used to accurately predict the DE of aluminum particles as a function of particle size.

Figure 2 shows the calculated DE prediction as a function particle size for pure Mg as well as AZ31B, ELE21, and WE43 alloys using helium gas as the accerlerating gas. The model predicts that pure Mg can be consolidated over a vast range of particle sizes. This has been shown by other researchers using commercially pure Mg powders. However, most strutcural applications require the use of alloying additions. In terms of cold spray consolidation, the increase in particle hardness and strength increases the critcal velocity, the required velocity to substantially deform each particle, which causes the DE of the process to drop drastically as the mean particle size increases. Based on the model predictions the target powder size is 30 µm or under to get maximum deposition efficiency. Theoretically, spraying particles that are larger than 30 µm will have a lower deposition efficiency. For example, when the diameter size is 70 µm deposition efficiency drops to 50%.

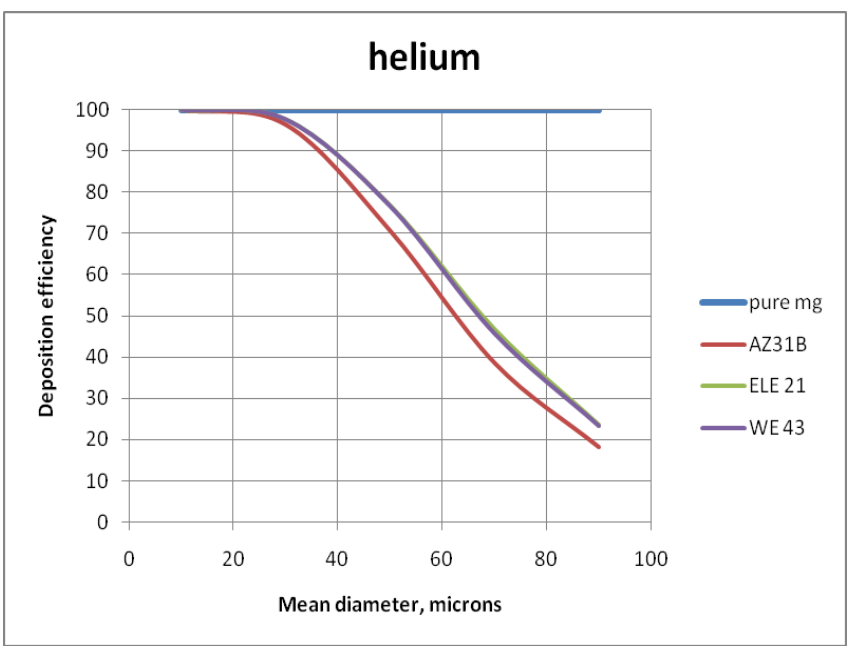

Figure 2: Model results showing calculated deposition efficiencies as a function of mean particle size

Powder characterization

Several batches of alloy powder were obtained for evaluation during this study. Inititially only ELE21 and WE43 were available with a mean particle size <150 μm. Finer powders were later obtained by sieving the coarse powders of ELE21, AZ31B and WE43. Starting powders were examined using scanning electron miscropscoy to identify powder morpholgy and relative size. Detailed particle size distribution (PSD) analysis was conducted using Horiba LA-910 laser scattering particle size distribution analyser. Cross sections of embedded AZ31B magnesium powder were obtained by mounting and polishing the powder suspension.

Cold spray deposition

Samples were sprayed using CGT 4000 system that was manipulated over the substrate using a 6-axis robot with helium as the carrying and driving gas. For AZ31B, samples were consolidated at five temperatures: 200, 250, 300, 350, & 400°C (392, 482, 572, 662, & 752°F) on 6061 Al substrates. The deposition efficiency (DE) was determined by calculating the ratio of weight gain to powder loss weight (5). After coatings were consolidated the samples were metallographically prepared and examined through optical microscopy. Quantitative image analysis was employed to determine microstructural characteristics such as percent porosity and percent undeformed particles. Vickers hardness measurements were also made to assess the relationship of gas temperature to mechanical deformation.

Results and Discussion

Figure 3 shows the microstructure of the initial consolidated ELE21 and WE43 powders. The large particle size of the powders prevented full densification as indicated by the large amount of interparticle voids and cracks. Likewise there is not a large amount of particle flattening which occurs once the critical velocity has been exceeded. Figure 4 shows the powder characteristics of finer powder procured after sieving

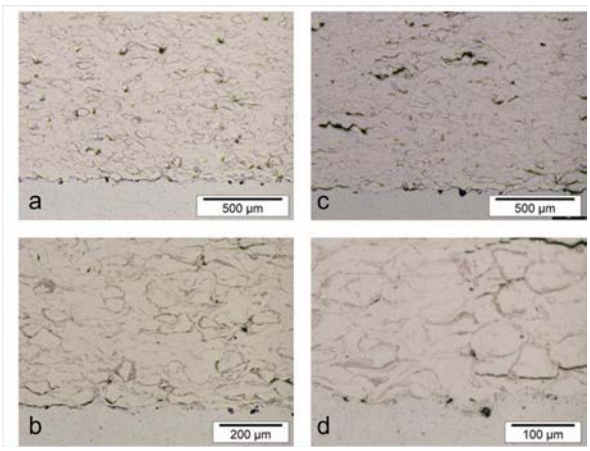

. Figure 3:SEM images of consolidated ELE21 (a&b) and WE43 (c&d) powders

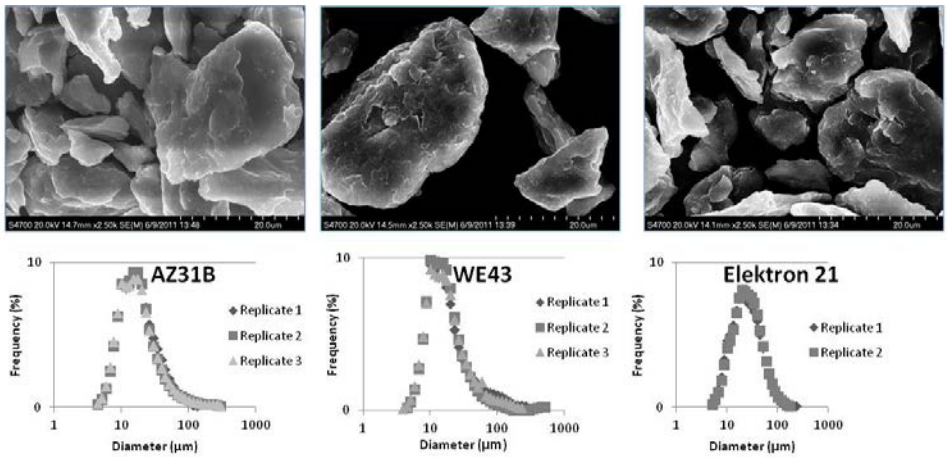

Figure 4:SEM images of powders and corresponding particle size distributions

In each case the mean particle diameter is below 30 mm. Based on the predicted DE model the reduction in particle size should enhance the consolidation process. The material characteristics of the deposits are summarized in Table 1.

TABLE 1: Characteristics of consolidated material

Powder	Porosity (Area %)	Average Hardness (VH)
AZ31B	2.52	135
ELE21	11.32	105
WE43	5.63	74

The porosity, as measured by image analysis, that exists in these samples is the product of individual large particles, as seen in the trailing edge of the PSD curves, not deforming and leaving voids in the consolidated material.

Based on these results a detailed parametric study was design centered on the material that exhibited the maximum densification, AZ31B. The mean diameter of the AZ31B powder was 21.3 ± 22.3 µm and 84.0% of the particles are under 29.9 µm. Figure 5 (a) shows a variety of asymetric geometries in a range of particle sizes typical of those found in ground powders. Figure 5 (b) presents a representative scanning electron micrograph which correlates with the PSD. Figure 5 (c) the polished samples show fully dense particles while Figure 5(d) shows no visible grain boundaries after etching. Figure 6 shows the resulting micrographs of AZ31B cold sprayed at a constant pressure at varying temperatures. Results of the characterization of the materials are found in Table 2.

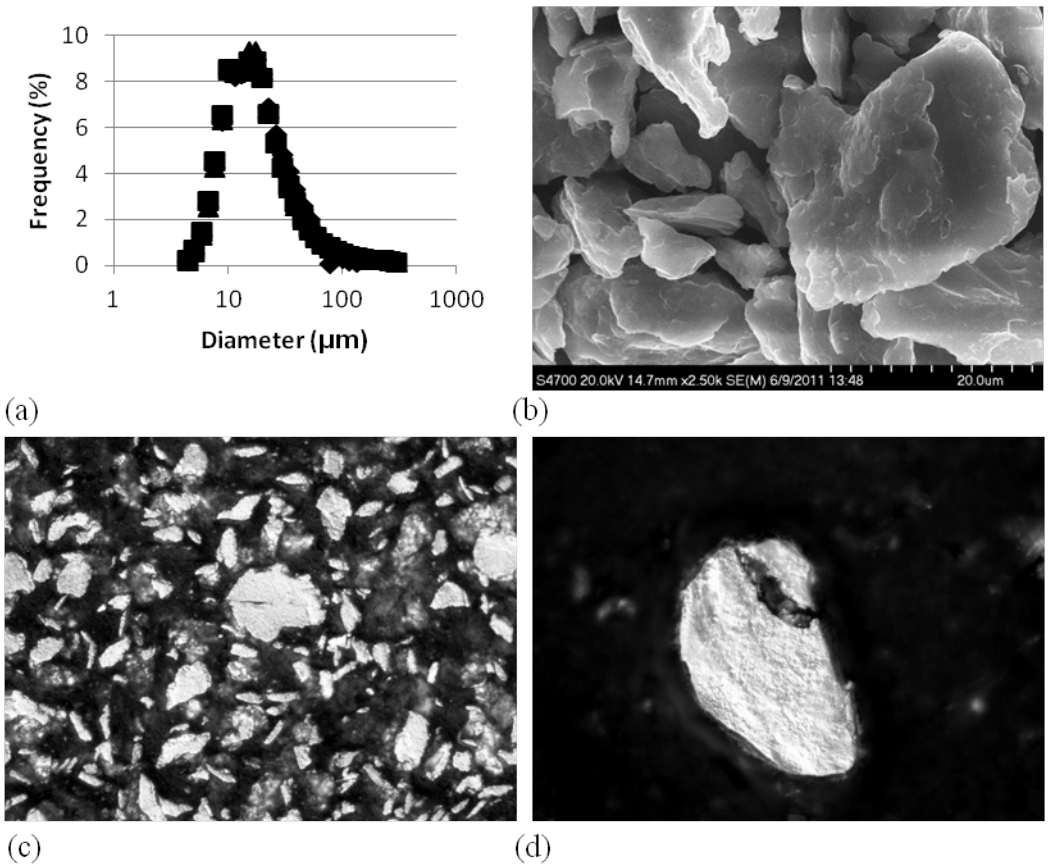

Figure 5 (a) Frequency (%) versus particle Diameter (µm) (b) electron micrograph of ground AZ31B powder (c) mounted and polished AZ31B powder (d) polished AZ31B alloy submerged for 15s in Acetic-Picral acid etchant.

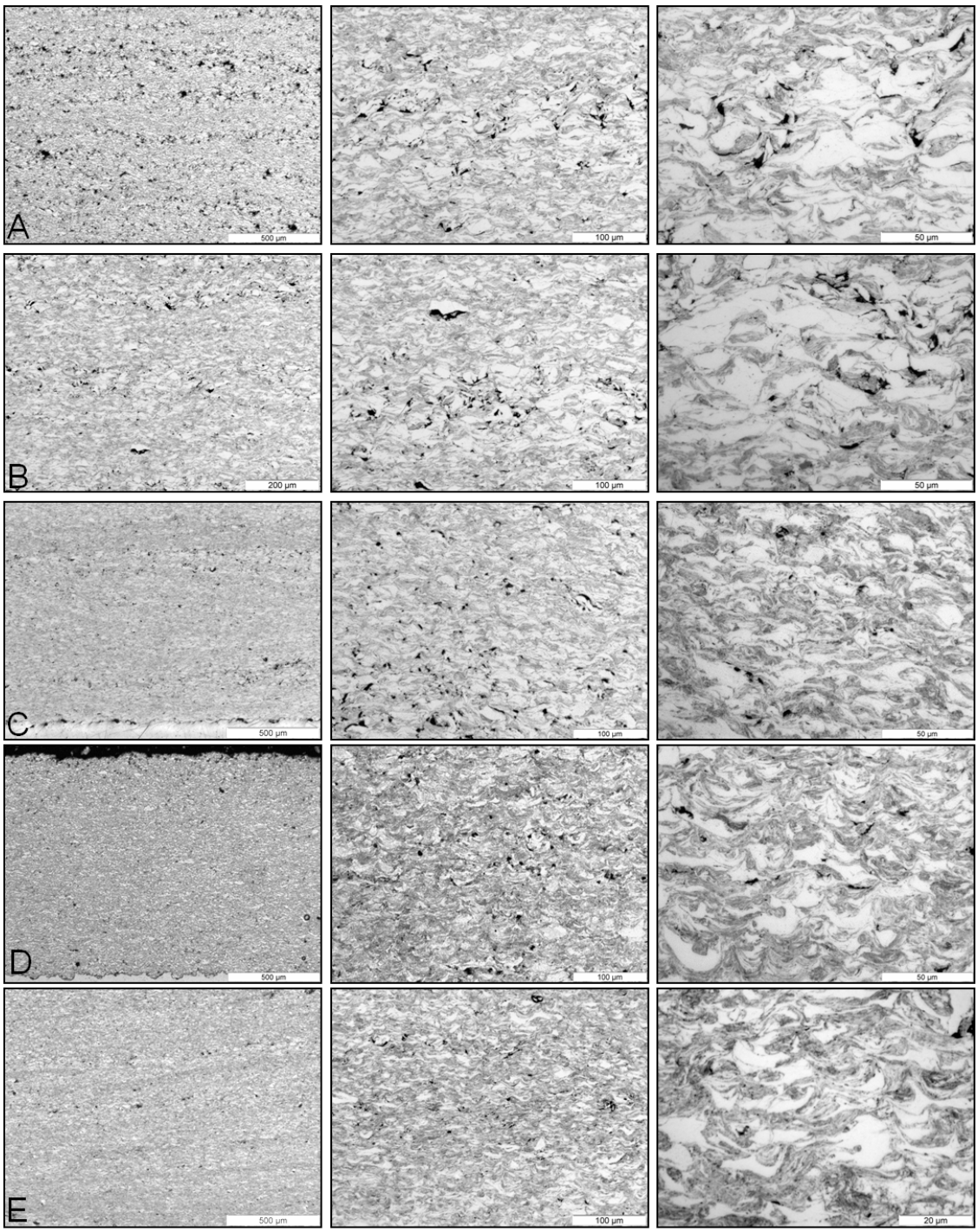

Figure 6. Representative micrographs of cold sprayed Magnesium alloy AZ31B. Row A: micrographs of 200 °C driving gas temperature. Row B: micrographs of 250°C. Row C: micrographs of 300 °C. Row D: micrographs of 350 °C. Row E: micrographs of 400°C.

Table 2: Porosity, Deposition Efficiency, Vickers hardness, Undeformed Particles of AZ31B

Temperature (°C)	Porosity (Area %)	Deposition Efficiency (DE) (%)	Average Hardness (VH)	Undeformed Particles (Area %)
200	5.41 (±0.24)	33.7	146.15 (±13.86)	25.57 (±4.97)
250	3.69 (±0.04)	37.2	159.15 (±9.30)	19.35 (±6.46
300	2.72 (±0.09)	41.1	161.48 (±13.52)	18.69 (±2.49)
350	0.88 (±0.51)	11.4	145.19 (±4.05)	13.49 (±2.64)
400	2.52 (±0.48)	30	134.83 (±11.16)	18.45 (±3.86)

As the driving gas temperature increases, the DE increases up to 300 °C then decreases as is shown in Figure 7a. Refering only to the phase diagram one would expect the trend to increase linearly until the eutectic point under which there is no change in the alloy. Further study is needed to determine what microstructural changes can occur as the powder temperature is increased. The decreased DE at elevated temperatures can be linked to increasing gas velocity that affects the flow pattern and can possibly create a slip stream above the substrate, which can impede powder substrate contact. The highest deposition efficiency was 41.7 % at 300 °C which was about 20% lower than theoretically calculated value. This discrepentcy is attributed to the fact that the model assumes spherical particle geometry whereas the ground powder used in this study has a more irregular morphology.

From Figure 7b the Vickers hardness measurement increases until 250 °C then remains constant within error up to 300 °C then decreases. Cold Spray involves plastic deformation known to increase hardness over other consolidation methods. The initial increase in hardness can be attributed to the higher amount of cold working at the lower temperatures that occurs during consolidation. The decrease in hardness after 300 °C can possibly be attributed to the higher mobility of dislocations and/or the occurrence of a microstructure change in the powder.

Porosity in Figure 7c is shown to have a negative slope to the driving gas temperature of 350 °C then becomes positive to 400 °C. This positive slope may be a result of oxidation between the layers of deposited material beyond a threshold temperature. The porosity occurs around undeformed particles therefore one would expect more porosity with more undeformed particles as seen in Figure 7d.

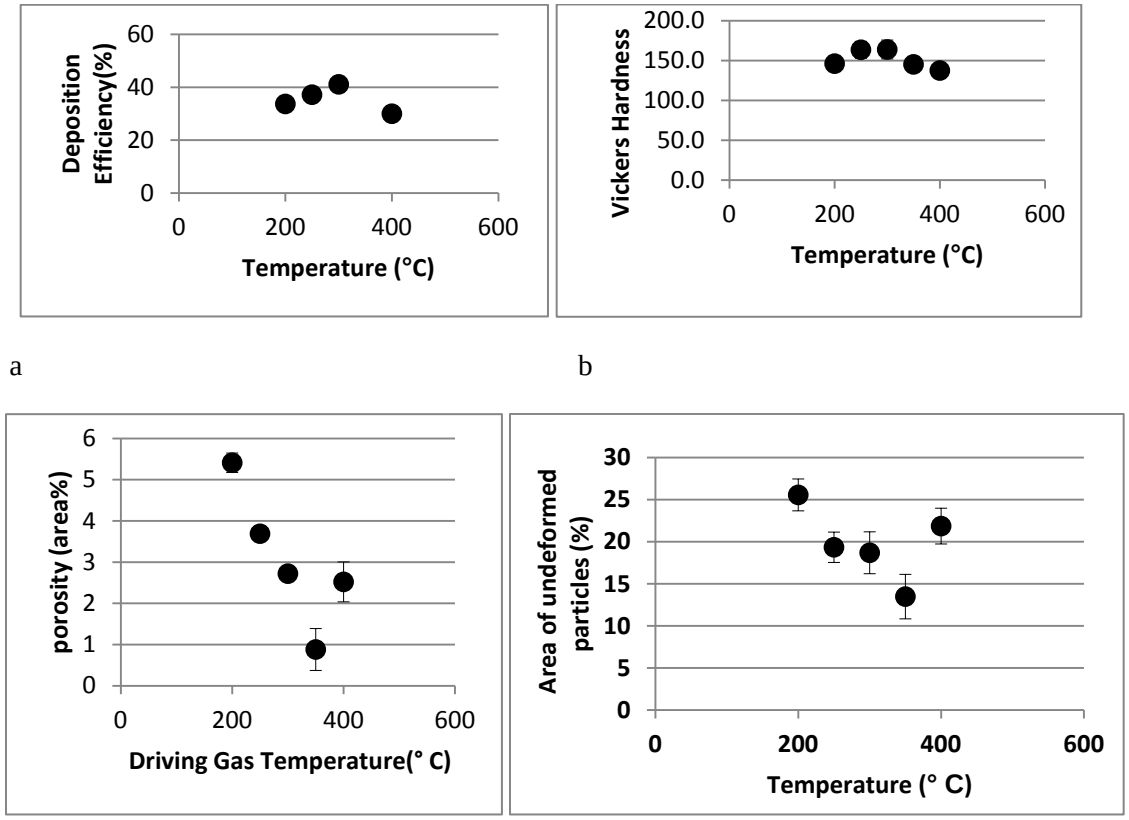

a b

c d

Figure 7 Material characteristics as a function of driving gas temperature

Conclusions

The cold spray process has been optimized using appropriate models and spray trials to consolidate Mg alloy powders. AZ31B, WE43 and ELE21 ground powders were consolidated and characterized in this work. The most successful consolidation occurs with AZ31B powder which was 97% full density. A temperature study showed that some softening effect or microstructural change occurs as the carrier gas temperature is increased above 300°C. Further characterization is planned to quantify this phenomenon.

References

1. *Microstructural effects of AZ31 magnesium alloy on its tensile deformation and failure behaviors.* **M. Marya, L. G. Hector, R. Verma, W. Tong.** 1-2, 2006, Materials science & Engineering A, Vol. 418, pp. 341-356.

2. *Interface Material Mixing Formed by the Deposition of Copper on Aluminum by Means of the Cold Spray Process.* **V.K. Champagne, D. Helfritch, P. Leyman, S. Grendahl, and B. Klotz.** 3, 2005, Journal of Thermal Spray Technology, Vol. 14, pp. 330-334.

3. *An Analysis of the cold Spray Process and Its Coatings.* **T. Stoltenhoff, H. Kreye, and H.J. Richter.** 4, 2001, Journal of Thermal Spray Technology , Vol. 11, pp. 542-550.

4. *Development of generalized parameter window for cold spray deposition.* **T. Schmidt, F. Gartner, H. Assadi, H. Kreye.** 1, 2005, Acta Materialia, Vol. 54, pp. 729-742.

5. *Particle Velocity and Deposition Efficiency in the Cold Spray Process.* **D.L. Gilmore, R.C. Dykhuizen, R.A. Neiser, T.J. Roemer, and M.F. Smith.** 1999, Journal of Thermal Spray Technology, pp. 576-582.